Supplemental Materials and Methods

Patient Fibroblast Culture

Patient fibroblasts were cultured at 37^{o}C, 5% CO_2 in DMEM (Gibco, 11995-065) supplemented with 10% FBS, 1% penicillin/streptomycin. Fibroblasts are seeded at 5x10^5 and allowed to reach 70-80% confluency prior to passages. For experiments, cells are serum starved in DMEM only for 48 hours to induce ciliogenesis. All cell lines used were within 1 passage number of each other and ≤10 total passages. All cell lines were routinely tested for mycoplasma.

CRISPR/Cas9 generation of *TOGARAM1* mut hTERT-RPE1 cell lines

hTERT-RPE1 were maintained in culture according to ATCC specifications. Cells were plated in 1 well of a 6 well plate. At ~70-80% confluency, cells were co-transfected with the Cas9 backbone px459v2 containing gRNAs to TOGARAM1. Transfections were performed with lipofectamine 2000 (Thermo Fisher). Sequencing primers for genotyping targeted the 5'UTR CTGAAGCTGTTCTTTTGCCTCT (forward) and exon 1 CTACCTCCTTCCACAAGCACTC (reverse). Both TOGARAM1 mut clone 1 and 2 have compound heterozygous mutations which result in large deletions including the ATG site and a portion of exon 1. *TOGARAM1* mut line 1: NM_001308120.2:c.[2_269del;270dup]; [2_269inv]. TOGARAM1 mut line 2: NM_001308120.2:c.[-33_314del]; [2_269inv; 269_270insTC] (Supplemental Figure 5 A, B). Cloning was performed as previously described (1). gRNAs to the 5'UTR and ATG site, 5'-CACCTGACAACCCTGCATGG-3' and exon 1, 5'-TCTGGAGGCGGTTTGTCAGG-3', were designed utilizing the web-based tool CHOPCHOP. pSpCas9(BB)-2A-Puro (PX459) V2.0 from Feng Zhang (Addgene plasmid # 62988) was purchased from Addgene.

hTERT-RPE1 Immunofluorescence and microscopy

Human telomerase-immortalized retinal pigment epithelium (hTERT-RPE1) cells were cultured according to ATCC specifications. For immunofluorescence imaging, cells were plated on glass coverslips. At 24 hr after plating, cells were serum starved for 48 hr in 0.2% FBS medium to induce cell cycle arrest and ciliogenesis. Transfections were performed where indicated at 48 hours post plating using lipofectamine 2000 (Thermo Fisher) in accordance with the manufacturer's protocol. 72 hours after plating, cells were rinsed once with 1X PBS, fixed with 2% paraformaldehyde for 20 min and permeabilized with 1% Triton-X for 5 min. All steps were performed at room temperature. Cells were blocked in freshly prepared 2% BSA for 45 min and then incubated with the following antibodies for 1 hr: rabbit polyclonal anti-ARL13B (Proteintech, cat. no. 17711-1-AP; 1:500), guinea pig polyclonal anti-RPGRIP1L (in house; SNC040, 1:300), monoclonal anti-acetylated tubulin antibody (clone 6-11-B1, Sigma-Aldrich, cat. no. T6793; 1:1,000), monoclonal anti-GT335 (a kind gift from Carsten Janke; 1:2000), rabbit polyclonal anti-SMO (Abcam, cat. no. ab38686; 1:200), and mouse monoclonal anti-ARL13B (NeuroMab, cat. no. 75-287; 1:500). Cells were stained with secondary antibodies for 45 min. The following secondary antibodies were used (all from Life Technologies/Thermo Fisher Scientific; all diluted 1:500 in 2% BSA): anti-guinea pig IgG Alexa Fluor 647, anti-rabbit IgG Alexa Fluor 488, and anti-mouse IgG Alexa Fluor 568. Fluoromount-G mounting solution with DAPI (ThermoFisher) was used to mount the coverslips to slides. Non-confocal imaging was performed with the Zeiss Axio Imager Z2 Microscope. Confocal imaging was done with the Zeiss LSM 880 Laser scanning microscope equipped with Airyscan technology.

Fixation and staining for patient fibroblast immunofluorescence

Patient fibroblasts were grown on coverslips (Neuvitro, GG-12-1.5.pdl, 0.3mg/mL Poly-D-lysine coating, 1.5mm thickness), serum-starved for 48 hours, then fixed in ice cold 2% paraformaldehyde in PBS for 20 minutes. After a PBS wash, cells were permeablized with 1% Trition-X in PBS or ice-cold Methanol for 5 minutes. Cells were blocked in 2% BSA in PBS for 1 hour at room temperature, then incubated with the

following antibodies (in 2% BSA/PBS) for 1.5 hours at room temperature: mouse anti-polyglutamylated tubulin, GT335, (Adipogen, AG- 20B-0020-C100, 1:2000), mouse anti-acetylated tubulin (clone 6-11-B1, Sigma-Aldrich, T6793; 1:1,000), mouse anti-ARL13B (UC Davis NeuroMab 75-287 clone N295B/66, 1:2000), goat anti-γ-tubulin (Santa Cruz, SC-7396 1:200), rabbit anti-ARL13B (Proteintech, 17711-1-AP, 1:200), or rabbit anti-INPP5E (Proteintech, 17797-1-AP, 1:100). Cells were washed thrice with PBS and stained with secondary antibodies (in 2% BSA/PBS) for 1 hour at room temperature (all Invitrogen at 1:2000, anti-goat-647, A21447, anti-rabbit-488, A11008). After three PBS washes, coverslips were mounted on slides using Fluoromount-G with DAPI (Invitrogen, 00-4959-52) and sealed with nail polish.

Patient Fibroblast Microscopy & Immunofluorescence Quantification

Wide-field fluorescent images were acquired on an 3i imaging workstation (3i, Denver, CO) with Axio inverted microscope with Definite Focus (Zeiss). For each experiment, optimal exposures were determined for each fluorophore to ensure that we used the full dynamic range of our CoolSnap HQ2 camera (Photometrics, Inc., Tuscon, AZ) without saturating any pixels. Dark field correction was applied to each channel to remove artifacts generated from the camera and electronics due to non-uniformities in illumination. Z-stack images with 0.3 µm steps were acquired at ≥10 distinct locations on each slide with a 40x objection using identical scope settings for all slides in an experiment. Sum projected images were analyzed in FIJI (NIH). A reference ciliary mask was drawn atop the reference signal for each cilium by standardized methods. A skeleton measurement of this mask extracted ciliary length data. The average fluorescence intensity was measured within the cilium mask in the channel of interest. To correct for antibody background, the background from a region directly adjacent to each cilium was measured and subtracted.

Patient Fibroblast Cell Cycle Reentry Analysis

Near confluent cells were serum starved for 48 hours, then serum was added back for 0, 4, 8, 16, or 24 hours. Cells were tryspinzed, concentrated, then triturated in 10mg/mL DAPI and 0.1% nonident P-40 solution with a 25 gauge needle to release intact nuclei. Nuclear DNA content was measured with a 405 nm laser on a LSRII (BD Bioscience) flow cytometer, then data was analyzed in FCS Express 6 (De Novo Software) (2).

Zebrafish experiments: Phylogeny and Synteny Analysis, CRISPR gene editing, Scanning electron microscopy and Immunofluorescence

Phylogeny and Synteny analyses were performed as previously described (3), using the Phylogeny.fr platform (http://www.phylogeny.fr/) and the synteny database (http://syntenydb.uoregon.edu/synteny_db/). Briefly, for Phylogeny, length of input sequences varied between 256 (*xenopus* truncated version) and 516 amino acids, and after curation 487 amino acids were used for further analysis. For Synteny analysis, parameters were adjusted to sliding window sizes between 25 and 100, and several genes in the vicinity of TOGARAMs were used for additional syntenic comparison. Zebrafish (*Danio rerio*) were maintained at 28 °C with a 14 h/10 h light/dark cycle as previously described (4). All zebrafish protocols were in compliance with internationally recognized guidelines for the use of zebrafish in biomedical research, and the experiments were approved by local authorities (Veterinäramt Zürich TV150). Generation and genotyping of the *armc9* mutant zebrafish was previously described (5). sgRNAs for *togaram1* CRISPR/Cas9 mutagenesis were designed with the website CHOPCHOP: 3'-GGGGTCTCCTCTGCTGGGCC-5' and 5'-GGACGAGATGCTGGACCGAG-3' for exon 6/7 and 3'-GGCTGCCGATGACCAGAGCT-5' and 5'-GGTGAATCTGCGCGCTCTGG-3' for exon 21/22 in *togaram1.* sgRNAs were mixed with Cas9 protein (gift from Darren Gilmour, M0646M NEB, or B25641 invitrogen) and co-injected into 1-cell stage embryos using a microinjector (Eppendorf). Amplification of the target regions for genotyping was performed using primer pairs 5'-AGACGCTCCTCAACTCCAGA-3' and 5'-

GCCGTGTAGACGAGTGTGTT-3' for exon 21/22 in *togaram1.* The PCR products were analyzed with gel electrophoresis and subcloned before sequencing. Experiments were performed using the *armc9*^{zh505} (WIK background) and the *togaram1*^{zh509} or *togaram1*^{zh510} (Tü background) mutants from generation F2+ (Supplemental Figure 6F). Zebrafish larvae were fixed in 2.5 % Glutaraldehyde in 0.1 M Cacodylate buffer and prepared for scanning electron microscopy (SEM) following standard protocols. SEM was performed on a ZEISS Supra VP 50 microscope. Whole-mount immunohistochemistry was performed on zebrafish larvae fixed in 4% paraformaldehyde or 80% MeOH in DMSO according to standard protocols. The following primary antibodies were used: acetylated tubulin (1:400, Sigma 7451), GT335 (1:400, Enzo Life Sciences A20631002), arl13b (1:100, gift from Z.Sun (6)), cc2d2a (7). Images were taken with a Leica HCS LSI confocal microscope. Acetylated tubulin and glutamylated tubulin mean fluorescence intensity was quantified using FIJI: fluorescence intensity of 10 cilia from each larvae were measured and averaged, so that each datapoint in graphs Fig 6A, 7E and 7F represents one individual larva. The background was subtracted from each measurement.

Cloning of constructs

All expression constructs were generated using Gateway Technology (Life Technologies) and according to manufacturer's instructions. The constructs generated encoded TOGARAM1 (and JBTS associated variants), ARMC9 (NM_025139.2),, pENTR223-CCDC66 (NM_001141947.3), CEP104 (NM_014704.4) and CSPP1 (NM_024790.6) in the following destination vectors: 3xHA, 3xFlag, TAP, myc, mRFP, GAL4-BD, and PalmMyr-CFP. The entry clone of human TOGARAM1 (NM_001308120.2) was synthesized and purchased from VectorBuilder. Constructs encoding TOGARAM1 and variants were generated by site directed mutagenesis PCR. All entry clone sequences were verified using Sanger sequencing.

PalmMyr Assay

hTERT-RPE1 cells were plated on glass slides, 24 hours later when cells reached approximately 80% confluency they were transfected using lipofectamine 2000 (ThermoFisher) with either mRFP-tagged TOGARAM1 / TOGARAM1 variants or PalmMyr-CFP-tagged ARMC9 or both. 24 hours post transfection, cells were starved for an additional 24 hours, fixed with 2% PFA at room temperature and prepared for analysis. Imaging was performed with the Zeiss Axio Imager Z2 Microscope.

Tandem affinity purification and mass spectrometry

HEK293Tcells were grown in DMEM (PAA) supplemented with 10% fetal bovine serum and 1% penicillin/streptomycin. Cells were seeded and expanded for 16 – 24 hours, then transfected with the corresponding SF-TAP-tagged DNA constructs using PEI reagent (Polysciences) according to the manufacturer's protocol. 48 hours later, cells were harvested in lysis buffer containing 0.5% Nonidet-P40 (NP-40), protease inhibitor cocktail (Roche), and phosphatase inhibitor cocktails II and III (Sigma-Aldrich) in TBS (30mM Tris-HCl, pH 7.4 and 150mM NaCl) for 20 min at 4°C. Cell debris and nuclei were removed by centrifugation at 10,000g for 10 min. For SF-TAP analysis, the cleared supernatant was incubated for 1 hour at 4°C with Strep-Tactin superflow (IBA). Subsequently, the resin was washed three times in wash buffer (TBS containing 0.1% NP-40 and phosphatase inhibitor cocktails II and III, Sigma-Aldrich). Protein baits were eluted with Strep-elution buffer (2mM desthiobiotin in TBS). For the second purification step, the eluates were transferred to anti-Flag M2 agarose beads (Sigma-Aldrich) and incubated for 1 hour at 4°C. The beads were washed three times with wash buffer and proteins were eluted with FLAG peptide (200 mg/ml, Sigma-Aldrich) in TBS. After purification, the protein samples were precipitated with chloroform and methanol and subjected to in-solution tryptic cleavage. Mass spectrometry and subsequent analysis were performed as previously described (8).

Yeast two-hybrid interaction analysis

The GAL4-based yeast two-hybrid system was used to screen for binary protein–protein interactions. Yeast two-hybrid constructs were generated according to manufacturer's instructions using Gateway cloning technology (Thermo Fisher Scientific) by LR recombination of GAL4-BD Gateway destination vectors with sequence verified Gateway entry vectors containing the cDNAs of selected bait proteins ARMC9, TOGARAM1, and CCDC66. Fragments thereof were generated by Gateway adapted PCR and subsequent cloning. Constructs encoding full-length or fragments of bait proteins fused to a DNA binding domain (GAL4-BD) were used as baits to screen human oligo-dT primed and bovine random hexamer primed retinal cDNA libraries, prey proteins are fused to a GAL4 activation domain (GAL4-AD). The yeast strain PJ96-4A, which carries the HIS3 (histidine), ADE2 (adenine), MEL1 (α-galactosidase) and LacZ (β-galactosidase) reporter genes, was used as a host. Interactions were analyzed by assessment of reporter gene (HIS3 and ADE2) activation via growth on selective media and β-galactosidase colorimetric filter lift assays (*LacZ* reporter gene). cDNA inserts of clones containing putative interaction partners were confirmed by Sanger sequencing.

Coimmunoprecipitation assay

HEK293T cells were plated in 6 well plates and transfected using Effectene Transfection Reagent (Qiagen) according to the manufacturer's protocol. Cells were subsequently incubated at 37^{o}C for 24 hours and then lysed in 200 µL per well of ice cold IP lysis buffer and collected for centrifugation. Lysates were centrifuged at 4 ^{o}C for 10 minutes at 11,000 rpm, supernatant was subsequently collected and incubated in new Eppendorf tubes with HA affinity matrix beads (Roche). Lysates were nutated for 2 hours at 4°C. The beads were spun down for 30 seconds at 4000 rpm. Beads were washed 3 times in 1 ml of ice cold IP lysis buffer, then all liquid was removed from the beads using a syringe with 0.5 mm needle. 50 µL of NuPAGE loading dye plus 100 mM DTT was added to the samples and they were heated at 95^{o}C for 10 minutes. Western blotting was performed using the standard protocol for the NuPAGE system and

visualized on the Odyssey. c-myc (Roche, 11667149001; 1:500), HA (Sigma; H9658; 1:1000), and Flag (Sigma; F3165-0.2MG; 1:1000) primary antibodies were used. The secondary antibody used was goat anti-Mouse IRDye800 (Licor biosciences; 926-32210; 1:20,000).

Western blotting

Trypsinized and concentrated cells were lysed with NP-40 cell lysis buffer (ThermoFisher, FNN0021). Cellular proteins were denatured using Laemmli sample buffer supplemented with 2-Mercaptoethanol (both BioRad, #1610747, #1610710) and heated at 95^{o}C for 10 minutes. Cellular proteins were separated by SDS-PAGE and transferred to a PVDF membrane (Millipore IPVH00010) using standard protocols. The following primary antibodies were used: mouse anti-acetylated tubulin (clone 6-11-B1, Sigma-Aldrich, T6793; 1:1,000), mouse-anti beta-actin (Sigma, A5441, 1:5000), rabbit anti-ARL13B (Proteintech, 17711-1-AP, 1:1000), rabbit anti-INPP5E (Proteintech, 17797-1-AP, 1:1000), rabbit anti-Giantin (Abcam, ab24586, 1:5000) or rabbit anti-ARMC9 (Atlas Antibodies cat# HPA019041, RRID: AB_1233489; 1:2000). Anti-ARMC9 recognizes an epitope at the N-terminal portion of the protein. Western blots were developed using anti-mouse or anti-rabbit secondary antibodies conjugated to horseradish peroxidase (anti-rabbit-HRP, Novex A16029 1:2000, anti-mouse-HRP, Invitrogen G21040 1:2000) and chemiluminescent substrate (BioRad Clarity Max 1705062). A ChemiDoc MP imaging system with ImageLab software was used for imaging (both BioRad).

Statistics and reproducibility

Statistical analyses were performed in Excel and Graphpad / Prism 6. Graphical data presented as percentages include 95% confidence intervals, but otherwise represent standard deviations. Quantitative immunofluorescence statistics were calculated with Student's t-test with unequal variances. Fluorescence intensity measurements from multiple experiments were combined for statistical analysis. Experiments

were independently performed thrice. In cilia stability assays, linear regression of ciliary loss over time yielded the slope, and we used Student's t-test with unequal variances for singular comparisons and a one-way ANOVA to assess significance for multiple samples. N values are stated in the figures and either represent cilia or cells (as indicated in each Figure). P values are stated in the figure legends, and symbols indicate the following P values: ns, $P > 0.05$; *, $P \leq 0.05$; **, $P \leq 0.01$; ***, $P \leq 0.001$; ****, $P \leq 0.0001$, *****, $P \leq 0.00001$.

Microtubule cold depolymerization assay

For microtubule cold depolymerization assays, cells were grown until near-confluent on coverslips in 24-well plates, serum starved for 48 hours, then placed at either room temperature or 4^{o}C for 10 minutes. Cells were then fixed as described and processed for immunofluorescence to determine ciliation percentage.

Cilia stability assay

For cilia stability assays, cells were grown until near-confluent on coverslips in 24-well plates, serum starved for 48 hours, then media was replaced with DMEM 10% FBS at hourly time points for 4-8 hours (9). Cells were then fixed as described and processed for immunofluorescence to determine ciliation percentage. In a subset of these experiments, we blocked histone deacetylase 6 (HDAC6) activity, with a specific inhibitor, tubacin (Sigma, SML0065). Cells were either treated with 1 μM tubacin in DMSO or in DMSO only as a vehicle control.

Subject Ascertainment and Phenotypic Data

The UW351 and UW360 families were enrolled under approved human subjects research protocols at the University of Washington (UW). The 13DG1578 family was enrolled King Faisal Specialist Hospital and

Research Centre KFSHRC RAC# 2070023, 2080006 and 2121053. The JAS-L50 family was enrolled in the 100,000 Genomes Project. All participants in the 100KGP have provided written consent to provide access to their anonymised clinical and genomic data for research purposes. The 100KGP research and clinical project model and its informed consent process has been approved by the National Research Ethics Service Research Ethics Committee for East of England – Cambridge South Research Ethics Committee. The WGL-191 family consented under a human subjects research protocol approved by the Ethics Committee at Tehran University of Medical Sciences.

All participants or their legal guardians provided written informed consent. All participants have clinical findings of JBTS (intellectual impairment, hypotonia, ataxia, and/or oculomotor apraxia) and diagnostic or supportive brain imaging findings (MTS or cerebellar vermis hypoplasia). Clinical data were obtained by direct examination of participants, review of medical records, and structured questionnaires.

Variant Identification

To identify the UW351 and UW360 families, samples from individuals affected by JBTS were previously screened using a molecular inversion probes (MIPs) targeted capture (10). See Supplemental Table 4 for the target gene list (11-35). In samples without causal variants, exome sequencing was performed as previously described (36) using Roche Nimblegen SeqCap EZ Human Exome Library v2.0 capture probes (36.5 Mb of coding exons) and paired-end 50 base pair reads on an Illumina HiSeq sequencer. In accordance with the Genome Analysis ToolKit's (GATK) best practices, we mapped sequence reads to the human reference genome (hg19) using the Burrows-Wheeler Aligner (v.0.7.8), removed duplicate reads (PicardMarkDuplicates v.1.113), and performed indel realignment (GATK IndelRealigner v.3.1) and base-quality recalibration (GATK TableRecalibration v.3.1). We called variants using the GATK UnifiedGenotyper and flagged with VariantFiltration to mark potential false positives that did not pass the following filters: Heterozygous Allele Balance (ABHet) > 0.75, Quality by Depth > 5.0, Quality (QUAL) > 50.0, Homopolymer

Run (Hrun) < 4.0, and low depth (< 8x). We used SeattleSeq for variant annotation and the Combined Annotation Dependent Depletion (CADD) score to determine deleteriousness of identified missense variants (37). Based on CADD score data for causal variants in other JBTS-associated genes, we used a CADD score cutoff of 15 to define deleterious variants (26). In Supplemental Figure 3E, we used the Integrated Genome Viewer for visualization of next-generation sequencing data (38).

For family 13DG1578, DNA from the affected individual, unaffected siblings, and parents were genotyped using the Axiom SNP Chip platform to determine the candidate autozygome (39, 40). WES was performed using TruSeq Exome Enrichment kit (Illumina) following the manufacturer's protocol. Samples were prepared as an Illumina sequencing library, and then the sequencing libraries were enriched for the desired target using the Illumina Exome Enrichment protocol. The captured libraries were sequenced using an Illumina HiSeq 2000 Sequencer. The reads were mapped against UCSC hg19 by BWA. SNPs and indels were detected by SAMTOOLS. Homozygous rare, predicted-deleterious, and coding/splicing variants within the autozygome of the affected individual were considered as likely causal. We defined rare variants as those with frequency of <0.1% in publicly available variant databases (1000 Genomes, Exome Variant Server, and gnomAD) as well as a database of 2,379 in-house ethnically matched exomes, and defined deleterious if predicted to be pathogenic by PolyPhen, SIFT, and CADD (score > 15).

For family JAS-L50, whole genome sequencing was performed by Genomics England via the 100,000 Genomes Project using the Illumina TruSeq DNA PCR-Free sample preparation kit (Illumina, Inc.) and an Illumina HiSeq 2500 sequencer, generating a mean depth of 45x 10 (range from 34x to 72x) and greater than 15x for at least 95% of the reference human genome. WGS reads were aligned to the Genome Reference Consortium human genome build 37 (GRCh37) using Isaac Genome Alignment Software

(version 01.14; Illumina, Inc.). Sequence data was analysed using bcftools scripts designed to search vcf.gz files and individual BAM files were viewed using IGV.

For family WGL-1914, genomic DNA was extracted from whole blood. Human whole exome enrichment was performed using Twist Human Core Exome Plus Kit and the library was sequenced on an Illumina NovaSeq platform. Data analysis was performed using a standard clinical pipeline, and the homozygous TOGARAM1 variant was the only likely pathogenic variant identified that was consistent with the phenotype. The variant was validated by Sanger sequencing and confirmed heterozygous in parents.

Array CGH

To assess copy-number variation, we performed array comparative genomic hybridization using a custom 8x60K oligonucleotide array (Agilent Technologies) (41). For gene list see supplemental table 5. Probe spacing was a median of 11 bp in the exons, and a median of 315 bp throughout the intronic regions and 100 kb on either side of each gene. Data were generated on an Agilent Technologies DNA Microarray Scanner with Surescan High-Resolution Technology using Agilent Scan Control software and were processed and analyzed using Agilent Feature Extraction and Agilent Cytogenomics software. To determine the effect of the deletion in UW360-3, we extracted RNA (BioRad, Aurum Total RNA kit, 7326820) from the associated cell line and converted it to cDNA (Biorad, iScript Reverse Transcription Supermix, 1708840) for downstream Sanger sequencing. To determine segregation of this deletion in family UW360 and to determine the precise breakpoints, we amplified the deletion-flanking region from genomic DNA and Sanger sequenced.

References

1. Ran FA et al. Genome engineering using the CRISPR-Cas9 system. *Nat. Protoc.* 2013;8(11):2281–2308.
2. Rabinovitch PS. Chapter 18 DNA Content Histogram and Cell-Cycle Analysis. *Methods Cell Biol.* 1994;41(C):263–296.
3. Ojeda Naharros I et al. Loss-of-function of the ciliopathy protein Cc2d2a disorganizes the vesicle fusion machinery at the periciliary membrane and indirectly affects Rab8-trafficking in zebrafish photoreceptors. *PLoS Genet.* 2017;13(12):e1007150–32.
4. Mullins MC, Hammerschmidt M, Haffter P, Nüsslein-Volhard C. Large-scale mutagenesis in the zebrafish: in search of genes controlling development in a vertebrate. *Curr. Biol.* 1994;4(3):189–202.
5. Van De Weghe JC et al. Mutations in ARMC9, which Encodes a Basal Body Protein, Cause Joubert Syndrome in Humans and Ciliopathy Phenotypes in Zebrafish. *Am. J. Hum. Genet.* 2017;101(1).
6. Duldulao NA, Lee S, Sun Z. Cilia localization is essential for in vivo functions of the Joubert syndrome protein Arl13b/Scorpion. *Development* 2009;136(23):4033–4042.
7. Bachmann-Gagescu R et al. The ciliopathy gene cc2d2a controls zebrafish photoreceptor outer segment development through a role in Rab8-dependent vesicle trafficking. *Hum. Mol. Genet.* 2011;20(20):4041–4055.
8. Boldt K et al. An organelle-specific protein landscape identifies novel diseases and molecular mechanisms. *Nat. Commun.* 2016;7:1–13.
9. Postma FR et al. Serum-induced membrane depolarization in quiescent fibroblasts: activation of a chloride conductance through the G protein-coupled LPA receptor. *EMBO J.* 1996;15(1):63–72.
10. O'Roak BJ et al. Multiplex targeted sequencing identifies recurrently mutated genes in autism spectrum disorders. *Science.* 2012;338(6114):1619–1622.
11. Bielas SL et al. Mutations in INPP5E, encoding inositol polyphosphate-5-phosphatase E, link phosphatidyl inositol signaling to the ciliopathies. *Nat. Genet.* 2009;41(9):1032–1036.
12. Lee JE et al. CEP41 is mutated in Joubert syndrome and is required for tubulin glutamylation at the cilium. *Nat. Genet.* 2012;44(2):193–199.
13. Halbritter J et al. Defects in the IFT-B component IFT172 cause Jeune and Mainzer-Saldino syndromes in humans. *Am. J. Hum. Genet.* 2013;93(5):915–925.
14. Ferland RJ et al. Abnormal cerebellar development and axonal decussation due to mutations in AHI1 in Joubert syndrome. *Nat. Genet.* 2004;36(9):1008–1013.
15. Valente EM et al. Mutations in TMEM216 perturb ciliogenesis and cause Joubert, Meckel and related syndromes. *Nat. Genet.* 2010;42(7):619–625.
16. Edvardson S et al. Joubert syndrome 2 (JBTS2) in Ashkenazi Jews is associated with a TMEM216 mutation. *Am. J. Hum. Genet.* 2010;86(1):93–97.
17. Davis EE et al. TTC21B contributes both causal and modifying alleles across the ciliopathy spectrum. *Nat. Genet.* 2011;43(3):189–196.
18. Coene KLM et al. OFD1 is mutated in X-linked Joubert syndrome and interacts with LCA5-encoded lebercilin. *Am. J. Hum. Genet.* 2009;85(4):465–481.
19. Cantagrel V et al. Mutations in the Cilia Gene ARL13B Lead to the Classical Form of Joubert Syndrome. *Am. J. Hum. Genet.* 2008;83(2):170–179.
20. Arts HH et al. Mutations in the gene encoding the basal body protein RPGRIP1L, a nephrocystin-4 interactor, cause Joubert syndrome. *Nat. Genet.* 2007;39(7):882–888.
21. Baala L et al. The Meckel-Gruber syndrome gene, MKS3, is mutated in Joubert syndrome. *Am. J. Hum. Genet.* 2007;80(1):186–194.
22. Gorden NT et al. CC2D2A is mutated in Joubert syndrome and interacts with the ciliopathy-

associated basal body protein CEP290. *Am. J. Hum. Genet.* 2008;83(5):559–571.
23. Tuz K et al. Mutations in CSPP1 cause primary cilia abnormalities and Joubert syndrome with or without Jeune asphyxiating thoracic dystrophy. *Am. J. Hum. Genet.* 2014;94(1):62–72.
24. Srour M et al. Joubert Syndrome in French Canadians and Identification of Mutations in CEP104. *Am. J. Hum. Genet.* 2015;97(5):744–753.
25. Dafinger C et al. Mutations in KIF7 link Joubert syndrome with Sonic Hedgehog signaling and microtubule dynamics. *J. Clin. Invest.* 2011;121(7):2662–2667.
26. Bachmann-Gagescu R et al. Joubert syndrome: a model for untangling recessive disorders with extreme genetic heterogeneity. *J. Med. Genet.* 2015;52(8):514–522.
27. Garcia-Gonzalo FR et al. A transition zone complex regulates mammalian ciliogenesis and ciliary membrane composition. *Nat. Genet.* 2011;43(8):776–784.
28. Sang L et al. Mapping the NPHP-JBTS-MKS Protein Network Reveals Ciliopathy Disease Genes and Pathways. *Cell* 2011;145(4):513–528.
29. Thomas S et al. TCTN3 mutations cause Mohr-Majewski syndrome. *Am. J. Hum. Genet.* 2012;91(2):372–378.
30. Srour M et al. Mutations in C5ORF42 cause Joubert syndrome in the French Canadian population. *Am. J. Hum. Genet.* 2012;90(4):693–700.
31. Sayer JA et al. The centrosomal protein nephrocystin-6 is mutated in Joubert syndrome and activates transcription factor ATF4. *Nat. Genet.* 2006;38(6):674–681.
32. Romani M et al. Mutations in B9D1 and MKS1 cause mild Joubert syndrome: expanding the genetic overlap with the lethal ciliopathy Meckel syndrome. *Orphanet J. Rare Dis.* 2014;9(1):72.
33. Parisi MA et al. The NPHP1 gene deletion associated with juvenile nephronophthisis is present in a subset of individuals with Joubert syndrome. *Am. J. Hum. Genet.* 2004;75(1):82–91.
34. Lee JH et al. Evolutionarily assembled cis-regulatory module at a human ciliopathy locus. *Science.* 2012;335(6071):966–969.
35. Huang L et al. TMEM237 is mutated in individuals with a Joubert syndrome related disorder and expands the role of the TMEM family at the ciliary transition zone. *Am. J. Hum. Genet.* 2011;89(6):713–730.
36. Chong JX et al. The Genetic Basis of Mendelian Phenotypes: Discoveries, Challenges, and Opportunities. *Am. J. Hum. Genet.* 2015;97(2):199–215.
37. Kircher M et al. A general framework for estimating the relative pathogenicity of human genetic variants. *Nat. Genet.* 2014;46(3):310–315.
38. Robinson JT et al. Integrative Genome Viewer. *Nat. Biotechnol.* 2011;29(1):24–6.
39. Alkuraya FS. Autozygome decoded. *Genet. Med.* 2010;12(12):765–771.
40. Alkuraya FS. Discovery of Rare Homozygous Mutations from Studies of Consanguineous Pedigrees. *Curr. Protoc. Hum. Genet.* 2012;75(1):6.12.1–6.12.13.
41. Mefford HC et al. Rare copy number variants are an important cause of epileptic encephalopathies. *Ann. Neurol.* 2011;70(6):974–985.

Supplemental Figures

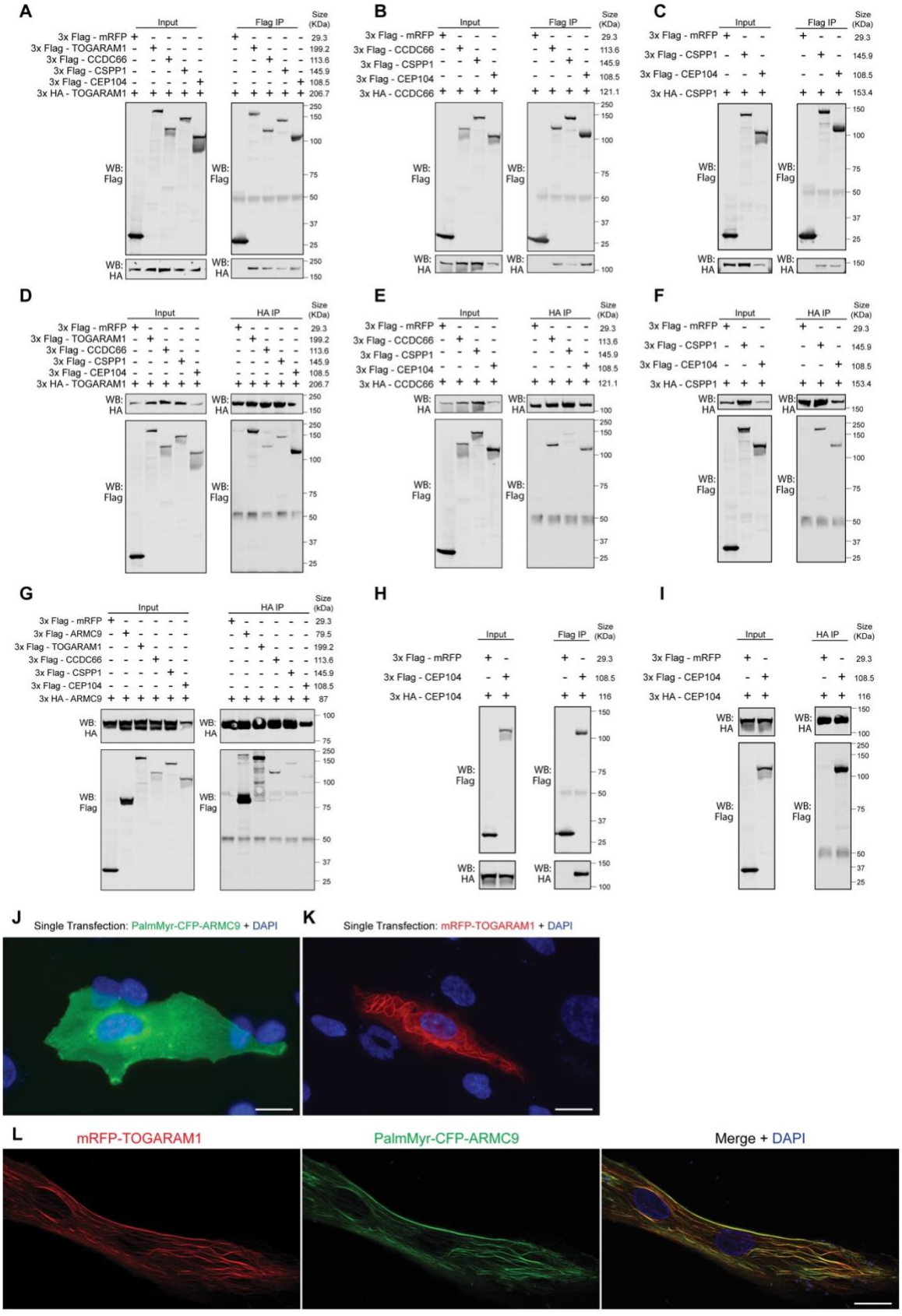

Supplemental Figure 1 Validation of ARMC9 interactome. **(A-I)** Reciprocal co-IPs of 3xFlag-ARMC9, 3xFlag-TOGARAM1, 3xFlag-CCDC66, 3xFlag-CSPP1, and 3xFlag-CEP104 with 3xHA-ARMC9, 3xHA-TOGARAM1, 3xHA-CCDC66, 3xHA-CSPP1, and 3xHA-CEP104. 3xFlag-mRFP was used as a negative control in each experiment. Pairs of Flag and HA tagged constructs were co-transfected into HEK293T cells, which were then lysed and subjected to pull down with either Flag or HA beads. Western blots of the pulldowns were probed with Flag and HA antibodies to visualize the interaction partners. The experiments were performed in triplicate. The reciprocal experiment of **(G)**, the Flag co-IP, is shown in Figure 1F. **(J-K)** Single transfections of PalmMyr-CFP-ARMC9 (green in **(J)**) and mRFP-TOGARAM1 (red in **(K)**) shows the localization of each tagged proteins in the absence of the other. **(L)** Co-expression of mRFP-TOGARAM1 and PalmMyr-CFP-ARMC9 shows localization consistent with a subset of cytoplasmic microtubules. Scale bar indicates 20 μm.

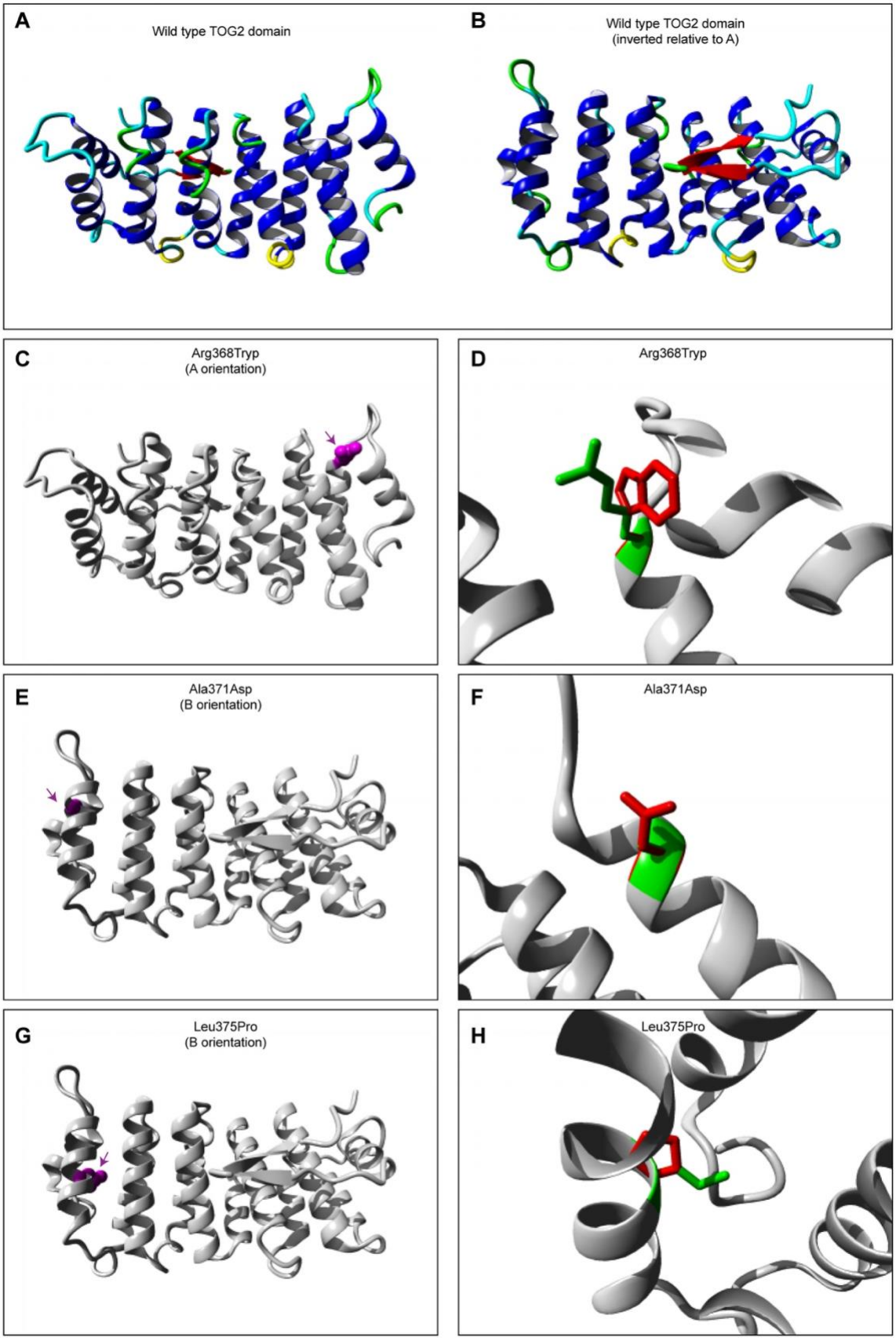
A
Wild type TOG2 domain
B
Wild type TOG2 domain
(inverted relative to A)
C
Arg368Tryp
(A orientation)
D
Arg368Tryp
E
Ala371Asp
(B orientation)
F
Ala371Asp
G
Leu375Pro
(B orientation)
H
Leu375Pro

Supplemental Figure 2 *In silico* modeling of the TOG2 variants. **(A-B)** Ribbon model (two views) of the wild-type TOGARAM1 TOG2 domain generated using HOPE. Alpha-helices are blue, beta-strand is red, turns are green, 3/10 helix is yellow, and random coil is cyan. (B) view is the inversion of wild-type TOGARAM1 TOG2 domain structure of as compared to (A) view **(C)** p. Arg368Trp missense variant in the TOG2 domain in ribbon-presentation generated using HOPE. **(D)** Close up of the side chain with wild-type arginine (green) and variant tryptophan (red). **(E)** p. Ala371Asp missense variant in the TOG2 domain. **(F)** Close up of the side chain with wild-type alanine (green) and variant aspartic acid (red). **(G)** p.Leu375Pro missense variant modeled in the TOG2 domain. **(H)** Close up of the side chain of both wild-type leucine (green) and variant proline (red). For (C, E, F) the TOG2 is shown in grey, the side chain of the mutated residue is shown in magenta. A magenta arrow indicates the location of the variant.

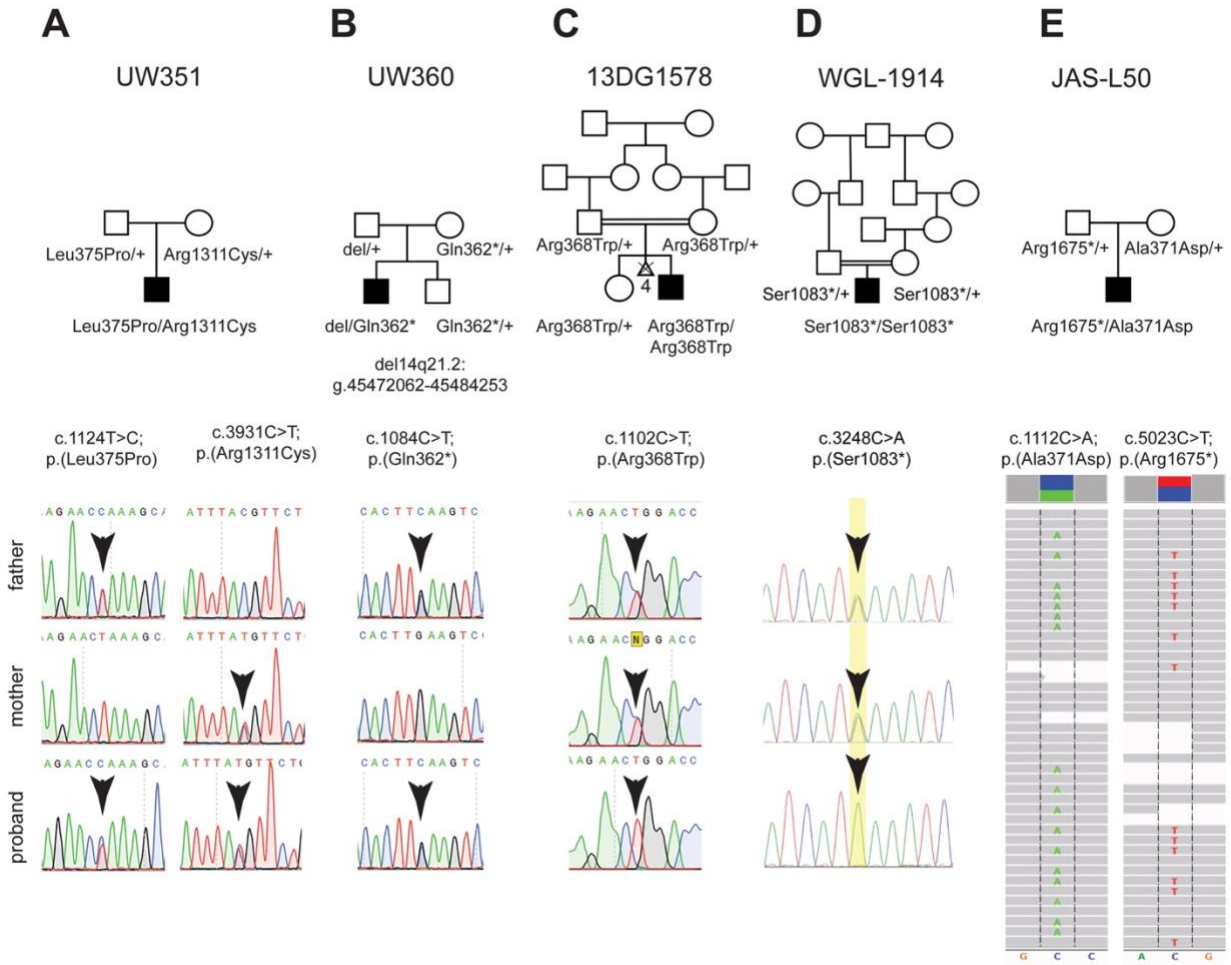

Supplemental Figure 3 Segregation and Sanger confirmation of *TOGARAM1* variants. **(A)** In UW351, Leu375Pro is inherited from father and Arg1311Cys is inherited from mother. **(B)** In UW360, Gln362* is inherited from mother and a multi-exon deletion is inherited from father. See Figure 2C for validation and paternal segregation of the deletion. **(C)** In 13DG1578, both parents are heterozygous for Arg368Trp and the proband is homozygous at this position. **(D)** In WGL-1914, both parents are heterozygous for Ser1083* and the proband is homozygous at this position. **(E)** In JAS-L50, Ala371Asp is inherited from the mother and the father was not available. Visualization of the next-generation sequencing data for the proband in the Integrated Genome Viewer confirms that the proband carries both pathogenic variants. Grey bars indicate individual reads with pathogenic variants in green and red; nucleotides at the bottom are the reference allele. Variants are indicated with arrows on the electropherograms.

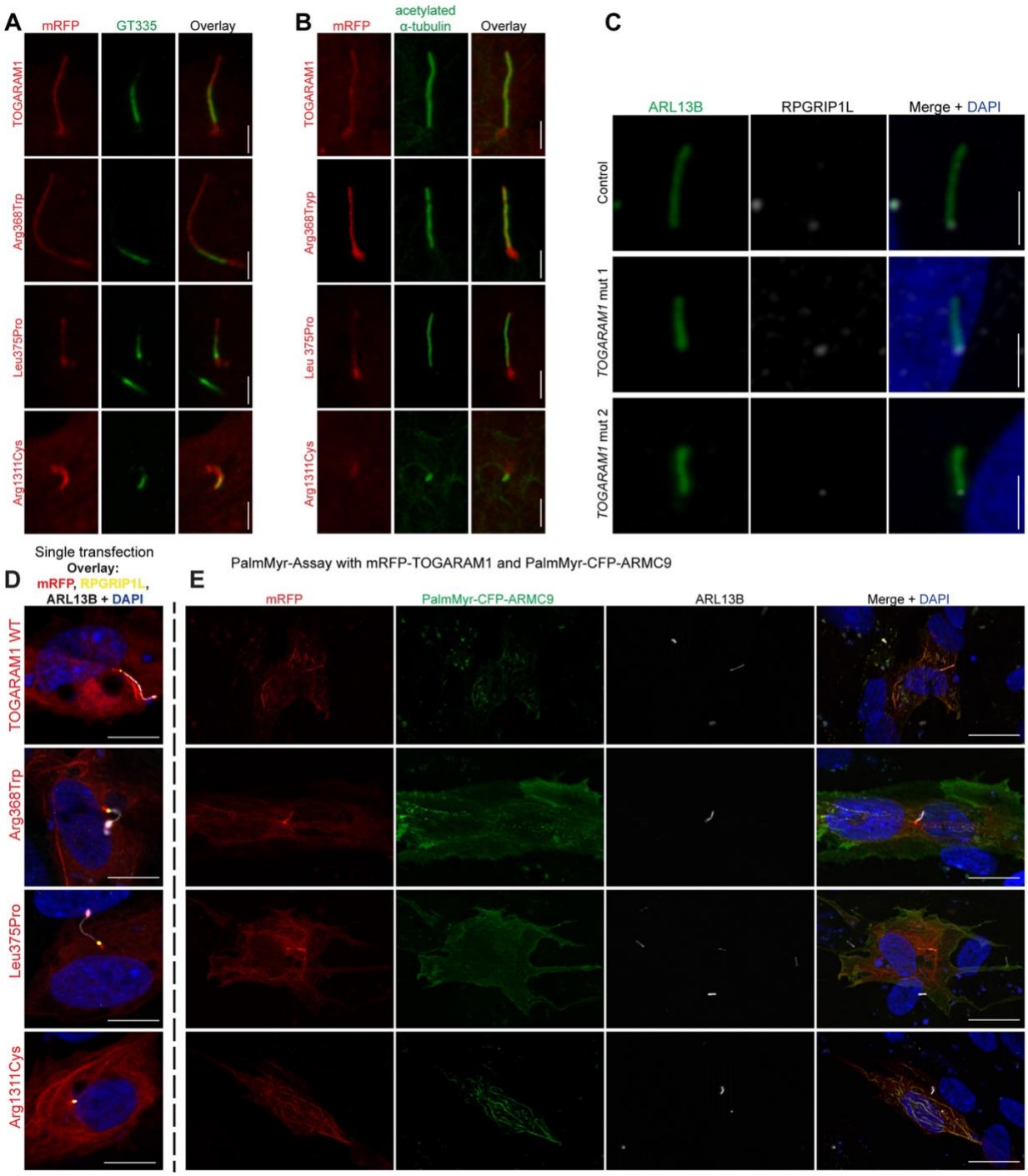

Supplemental Figure 4 Impact of *TOGARAM1* variants on localization, transition zone, and ARMC9 interaction **(A-B)** Wild-type and variant mRFP-tagged TOGARAM proteins co-localize with polyglutamylated (A) and acetylated tubulin (B) in transfected hTERT-RPE1 *TOGARAM1* mutant cells. GT335 antibody (green in (A)) marks the glutamylated portion of the ciliary axoneme and acetylated alpha-tubulin antibody (green in (B)) marks the entire ciliary axoneme. All images are representative of 3 independent imaging experiments. Scale bars are 2µm. **(C)** Images of cilia from control and engineered *TOGARAM1* mutant hTERT-RPE1 cell lines marked with ARL13B antibody (green, ciliary membrane) and

RPGRIP1L antibody (white, transition zone). Scale bars are 2µm. **(D)** PalmMyr assay with PalmMyr-CFP-ARMC9 and mRFP-TOGARAM1 expressed in control hTERT-RPE1 cells. Single transfections of mRFP-TOGARAM1 wild-type and variants show characteristic localization in the absence of PalmMyr-CFP-ARMC9 (mRFP (red), ARL13B (white), RPGRIP1L (yellow), and DAPI (blue)). Scale bar is 10µm. **(E)** Co-expression of mRFP-TOGARAM1 and PalmMyr-CFP-ARMC9 (mRFP (red), ARL13B (white), CFP (green), and DAPI (blue)). Wild-type and Arg1311Cys TOGARAM1 colocalize with PalmMyr-CFP-ARMC9, indicating an interaction, while Arg368Trp and Leu375Pro show little to no specific colocalization. Scale bar is 20µm.

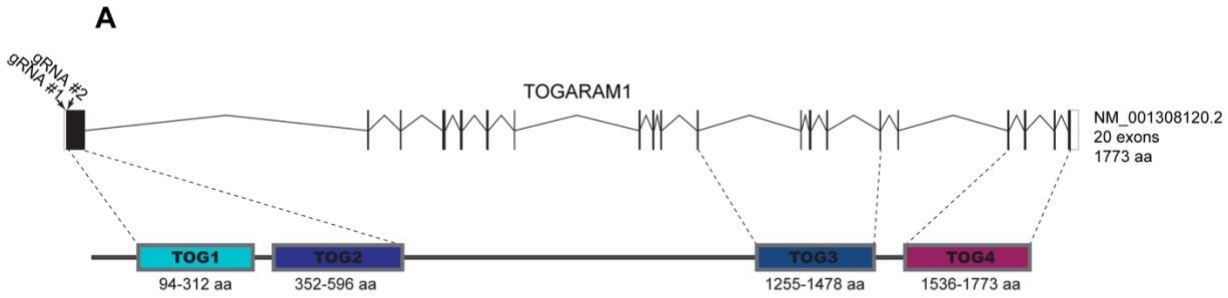

B

hTERT-RPE1 mut lines

NM_001308120.2	allele 1	allele 2
TOGARAM1 mut 1	c.[2_269del;270dup]	c.[2_269inv]
TOGARAM1 mut 2	c.[-33_314del]	c.[2_269inv; 269_270insTC]

Supplemental Figure 5 CRISPR/Cas9 edited *TOGARAM1* hTERT-RPE1 mutant lines. **(A)** Schematic representation of the TOG array aligned with the genomic region encoding *TOGARAM1*. The target sites of gRNA 1 and gRNA 2 are indicated by arrows in exon 1. They are predicted to cut at cDNA position 2 and 269 respectively. This portion of exon 1 encodes the region of the protein immediately before the TOG1 domain. **(B)** *TOGARAM1* mutant 1 harbors a 267 base pair deletion with a single base pair duplication in one allele and a 267 base pair inversion in the other allele, both occurring in exon 1: NM_015091.2:c.[2_269del;270dup]; [2_269inv]. *TOGARAM1* mutant line 2 harbors a 347 base pair deletion in one allele and a 267 base pair inversion with 2 base pair insertion in the other allele, both occurring in exon 1: NM_015091.2:c.[-33_314del]; [2_269inv; 269_270insTC].

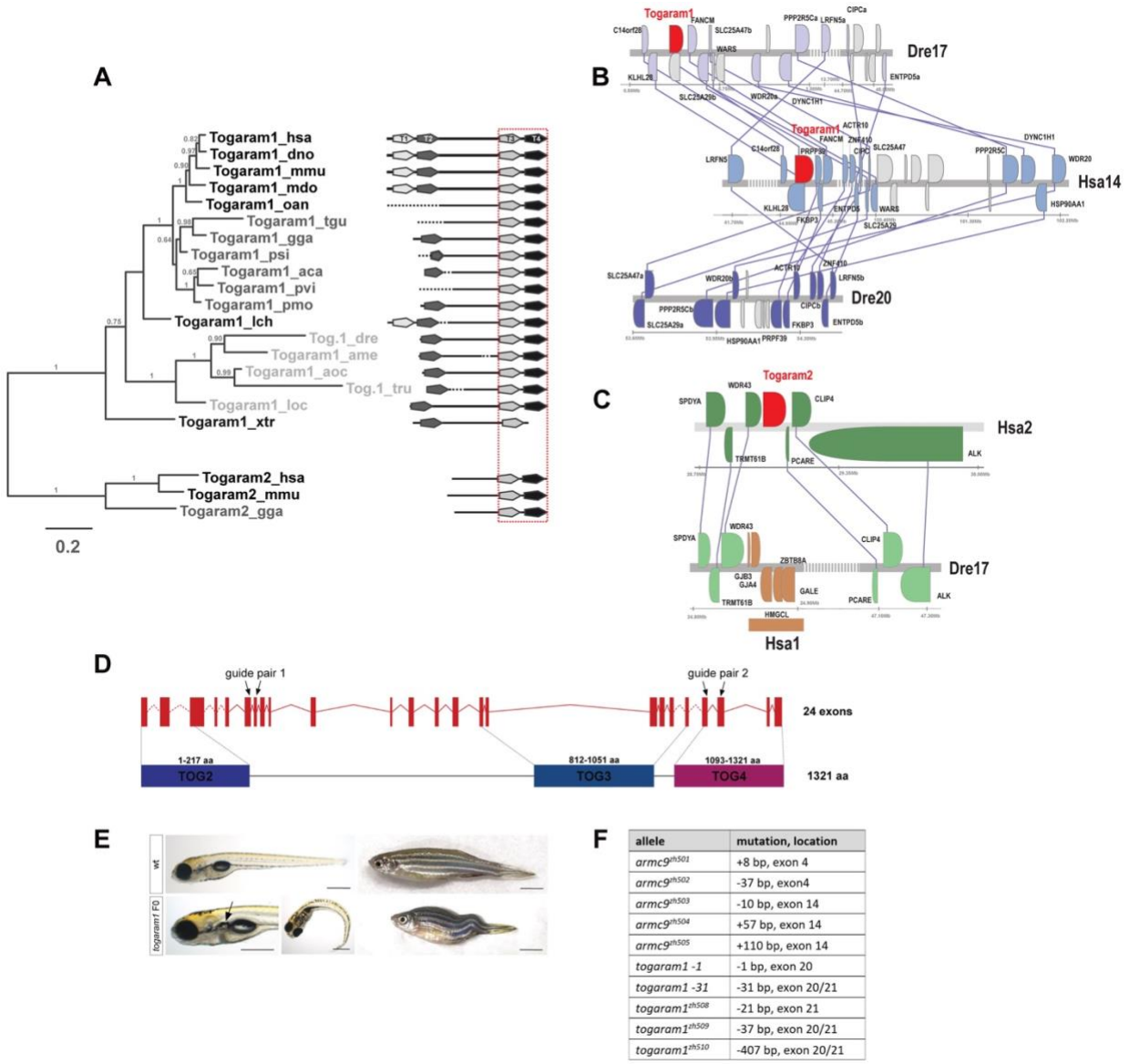

allele	mutation, location
armc9^{zh501}	+8 bp, exon 4
armc9^{zh502}	-37 bp, exon4
armc9^{zh503}	-10 bp, exon 14
armc9^{zh504}	+57 bp, exon 14
armc9^{zh505}	+110 bp, exon 14
togaram1 -1	-1 bp, exon 20
togaram1 -31	-31 bp, exon 20/21
togaram1^{zh508}	-21 bp, exon 21
togaram1^{zh509}	-37 bp, exon 20/21
togaram1^{zh510}	-407 bp, exon 20/21

Supplemental Figure 6 Togaram1 phylogeny, synteny and zebrafish F0 phenotypes. **(A)** Phylogenetic analysis of the C-terminal part (red box) of *TOGARAMs* in different vertebrate species revealed a clear phylogenetic separation of *TOGARAM1* and *TOGARAM2*. The following species were used for phylogeny: *Anolis carolinensis* (aca), *Astyanax mexicanus* (ame), *Amphiprion ocellaris* (aoc), *Dasypus novemcinctus* (dno), *Danio rerio* (dre), *Gallus gallus* (gga), *Homo sapiens* (hsa), *Latimeria chalumnae* (lch), *Lepisosteus oculatus* (loc), *Monodelphis domestica* (mdo), *Mus musculus* (mmu), *Ornithorhynchus anatinus* (oan), *Pelodiscus sinensis* (psi), *Pogona vitticeps* (pvi), *Taeniopygia guttata* (tgu), *Takifugu rubripes* (tru), *Xenopus tropicalis* (xtr). Dotted lines in the domain representation represent sequence strings so far not covered in the corresponding genome assemblies. In the phylogenetic tree mammals are given in black, amphibians, birds, turtles and reptiles in dark gray and teleosts in light gray. The scale bars represent the distance where 20% of the amino acids are changed. **(B)** Synteny analysis confirms orthology between human and zebrafish *TOGARAM1*. The human *TOGARAM1* gene is located on chromosome 14. Corresponding chromosomal regions to the human chromosome 14 are located on zebrafish chromosomes 17 and 20. In contrast to the zebrafish chromosome 17 where a *TOGARAM1* gene can be

readily identified, zebrafish chromosome 20 lacks a corresponding ortholog, suggesting that in the case of *TOGARAM1* no zebrafish duplicate of this gene has been retained. **(C)** Synteny analysis of human *TOGARAM2* shows no corresponding gene in zebrafish. Interestingly, no ortholog of human *TOGARAM2* (located on human chromosome 2) is present in the zebrafish genomic region where the genes flanking *TOGARAM2* are located. **(D)** Zebrafish *togaram1* exons and corresponding protein with domains. Red dashed lines represent unknown intron size. Location of sgRNAs for genome editing are indicated: two different sgRNAs per target region were co-injected to generate larger deletions. **(E)** Phenotype of *togaram1* F0 mosaic zebrafish: Larvae have kidney cysts (arrow) and body curvature. Adults develop scoliosis. Scale bars are 500µm for larvae and 5mm for adults. **(F)** Alleles generated with CRISPR/Cas9 for *armc9* and *togaram1*.

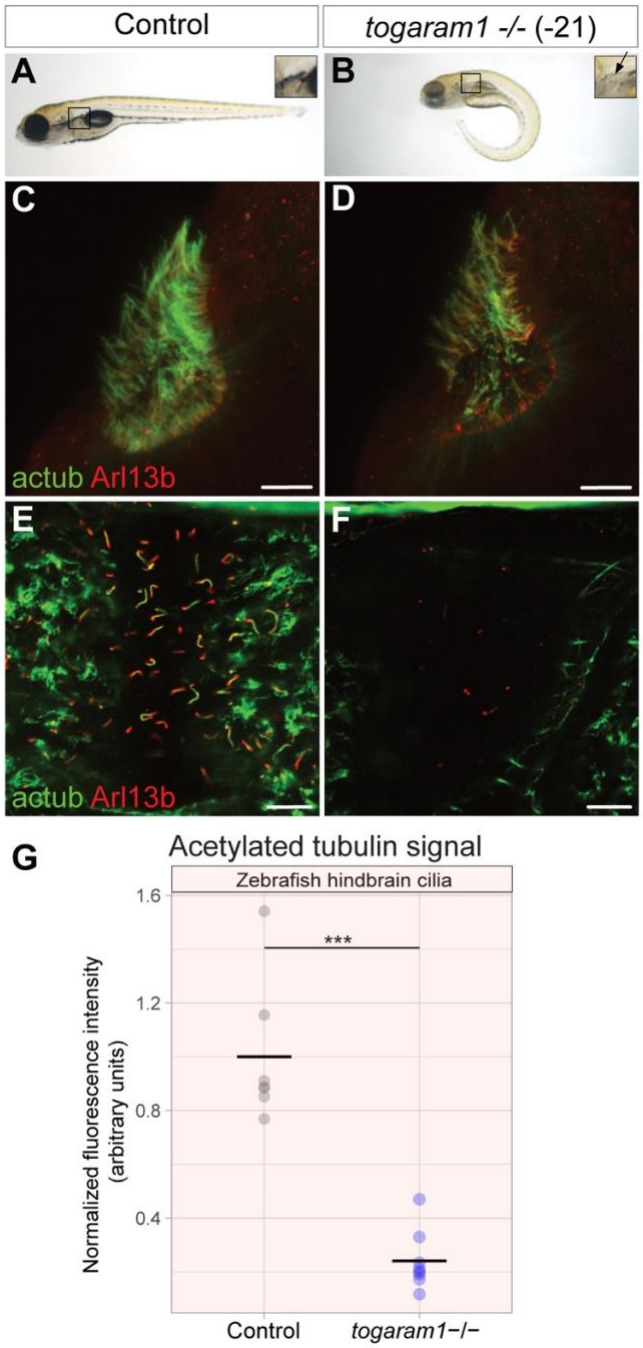

Supplemental Figure 7 Phenotypes of *togaram1*^{zh508} in-frame mutant zebrafish. **(A-B)** *togaram1*-/- (-21) larvae have kidney cysts and curved body shape compared to wild-type (A). Scale bars are 500µm. **(C-D)** Wild-type and **(D)** Acetylated tubulin (green) and Arl13b (red) immunofluorescence of 3 dpf *togaram1*-/- (-21) zebrafish nose pits shows decreased numbers of both motile and primary cilia compared to wild-type (C). **(E-F)** Acetylated tubulin (green) and Arl13b (red) immunofluorescence of hindbrain ventricles show a clear decrease in cilia number and acetylation in *togaram1*-/- (-21) compared to wild-type (E). Scale bars for (C-F) are 10µm. **(G)** Quantification of acetylated tubulin of cilia in hindbrain ventricles, $p<0.001$ using Student's t-test. Zebrafish controls are wt, +/+ or +/- siblings of -/-.

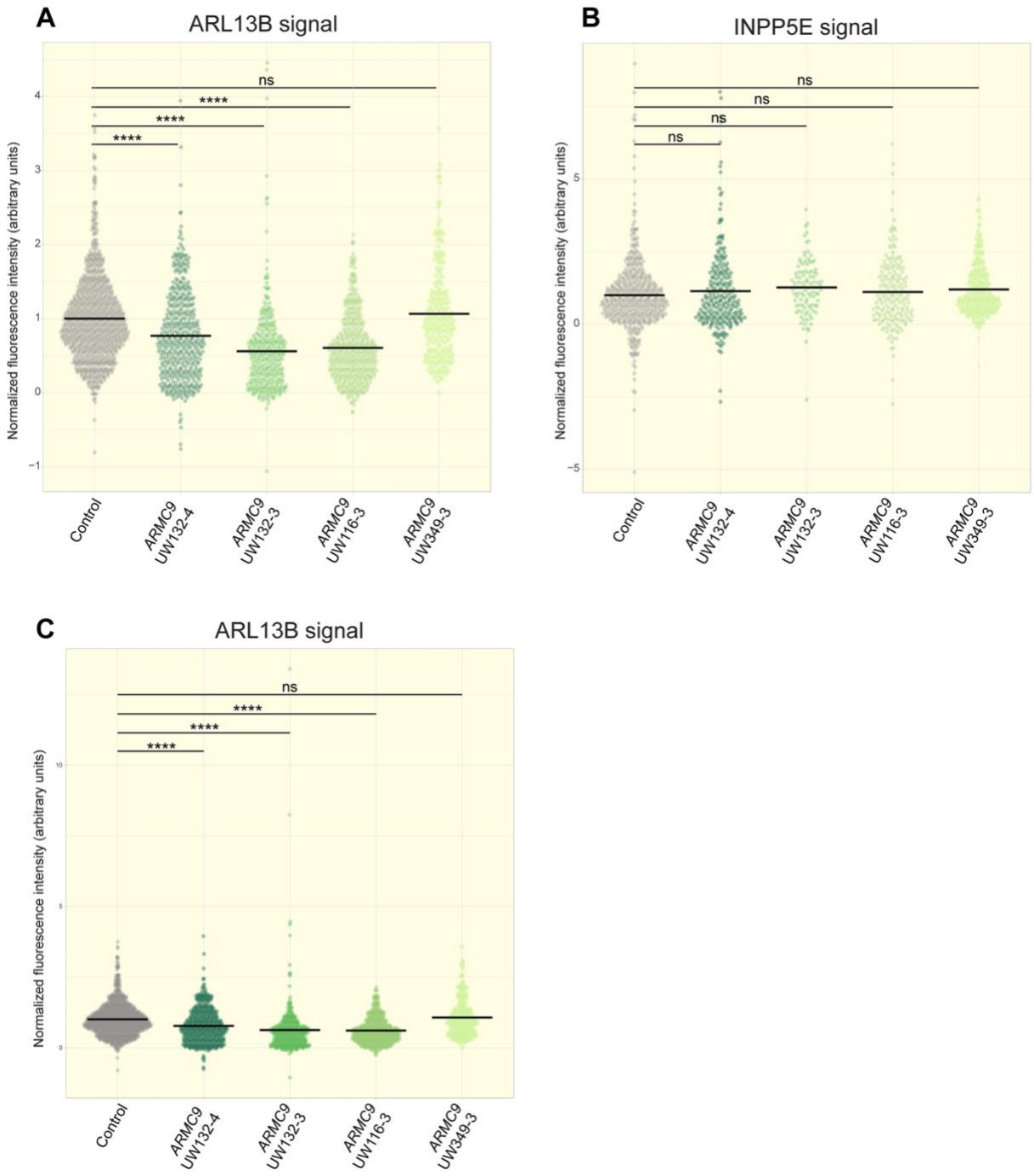

Supplemental Figure 8 Ciliary INPP5E levels are maintained across *ARMC9* patient fibroblast lines. **(A)** Normalized ciliary ARL13B fluorescence intensity in control and *ARMC9* patient fibroblasts. >200 cilia were assessed per line for measurements. (control = 935 cilia, UW132-4 = 472 cilia, UW132-3 = 337 cilia, UW116-3= 477 cilia, and UW349-3= 208 cilia). p<0.0001 between control and *ARMC9* patient cilia UW132-4, UW132-3, UW116-3, by one-way ANOVA and Dunnett's multiple comparison test. Results were not significant for control versus UW349-3 by one-way ANOVA. **(B)** Normalized ciliary INPP5E fluorescence intensity in control and *ARMC9* patient fibroblasts. >99 cilia were assessed per line for measurements. (control = 471 cilia, UW132-4 = 248 cilia, UW132-3 = 100 cilia, UW116-3= 180 cilia, and UW349-3= 194

cilia). Results were not significant as assessed by one-way ANOVA. Dunett's multiple comparison test yielded the following p values: control versus UW132-4 p= 0.4373, UW132-3 p=0.1701, UW116-3 p=0.7163, UW349-3 p=0.2038. **(C)** ARL13B intensity dataset including outlier data points that are not included in the other graphs, but are included in the statistical analyses. P-value symbols: ns $p>0.05$, ****$p\leq0.0001$. Bars represent the mean.

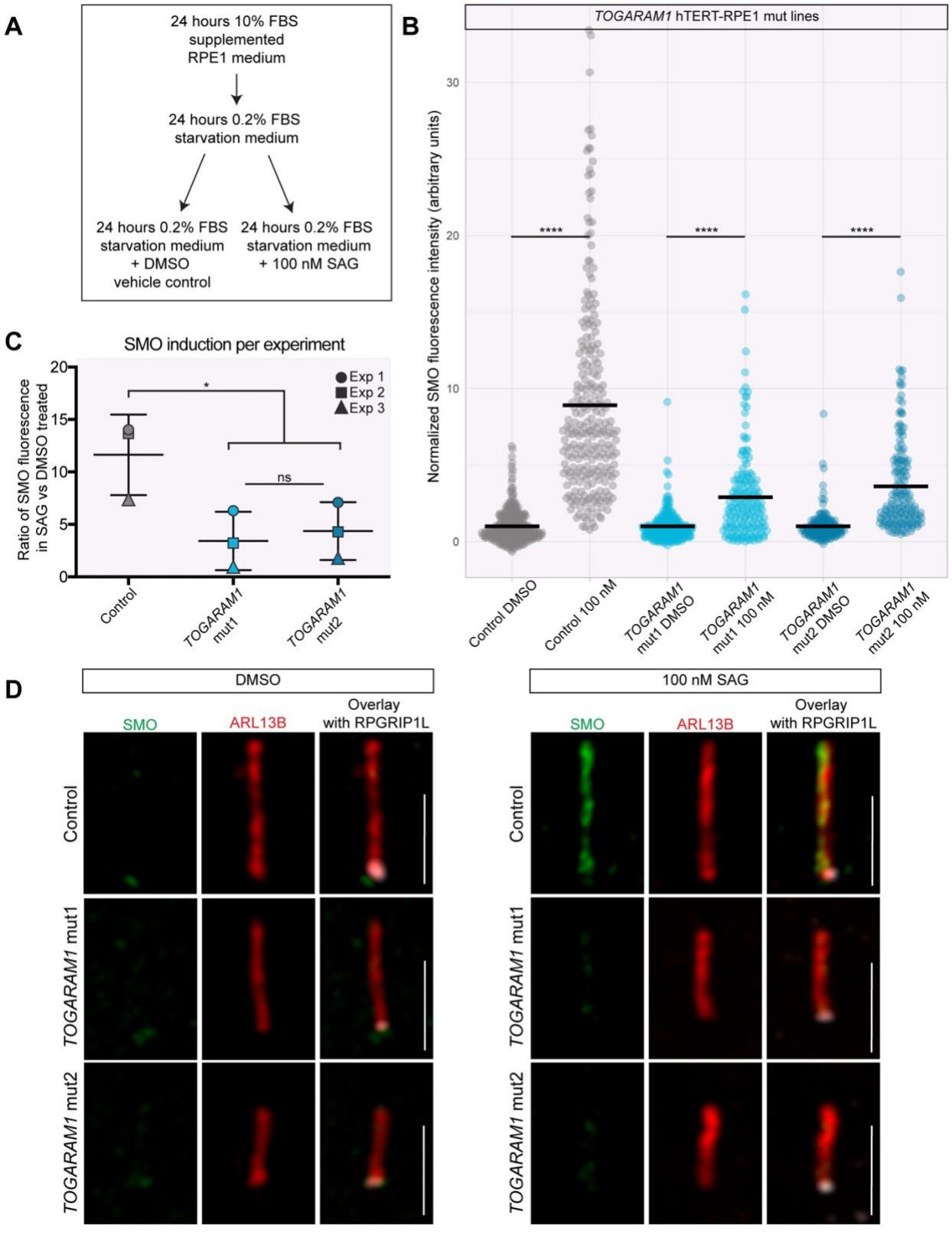

Supplemental Figure 9 SMO ciliary translocation is impaired in TOGARAM1 mutant cell lines. **(A)** Hh assay schematic. **(B)** Intensity values of SMO localization in the ciliary compartment between DMSO and 100

nM SAG treated control and TOGARAM1 mutant cell lines. >150 cilia were assessed for each condition and pooled from 3 independent experiments (For the control line, N=300 for DMSO and N=248 for SAG treatment, for TOGARAM1 mut1 N=210 for DMSO and N=165 for SAG treatment, and for TOGARAM1 mut2 N=157 for DMSO and N=162 for SAG treatment). Results were statistically significant as assessed by the Kruskal-Wallis test, multiple comparisons were corrected for using Dunn's test. $p<0.0001$ for DMSO versus 100 nM SAG treatment in all lines. **(C)** The median ratios of SMO induction levels in response to SAG treatment across experiments. The central bar represents the mean of 3 independent experiments, the error bars display the standard deviation. Results were statistically assessed by the Kruskal-Wallis test with Dunn's test for multiple testing correction. $p=0.02$ for induction of TOGARAM1 mut 1 line and TOGARAM1 mut 2 line versus induction in the control. No significant difference between the two *TOGARAM1* mutant lines was observed. **(D)** Representative immunofluorescence images of SMO (green) localization in DMSO and 100 nM SAG treated cells. ARL13B is shown in red (ciliary membrane) and RPGRIP1L is shown in white (transition zone). Scale bar is 2µm.

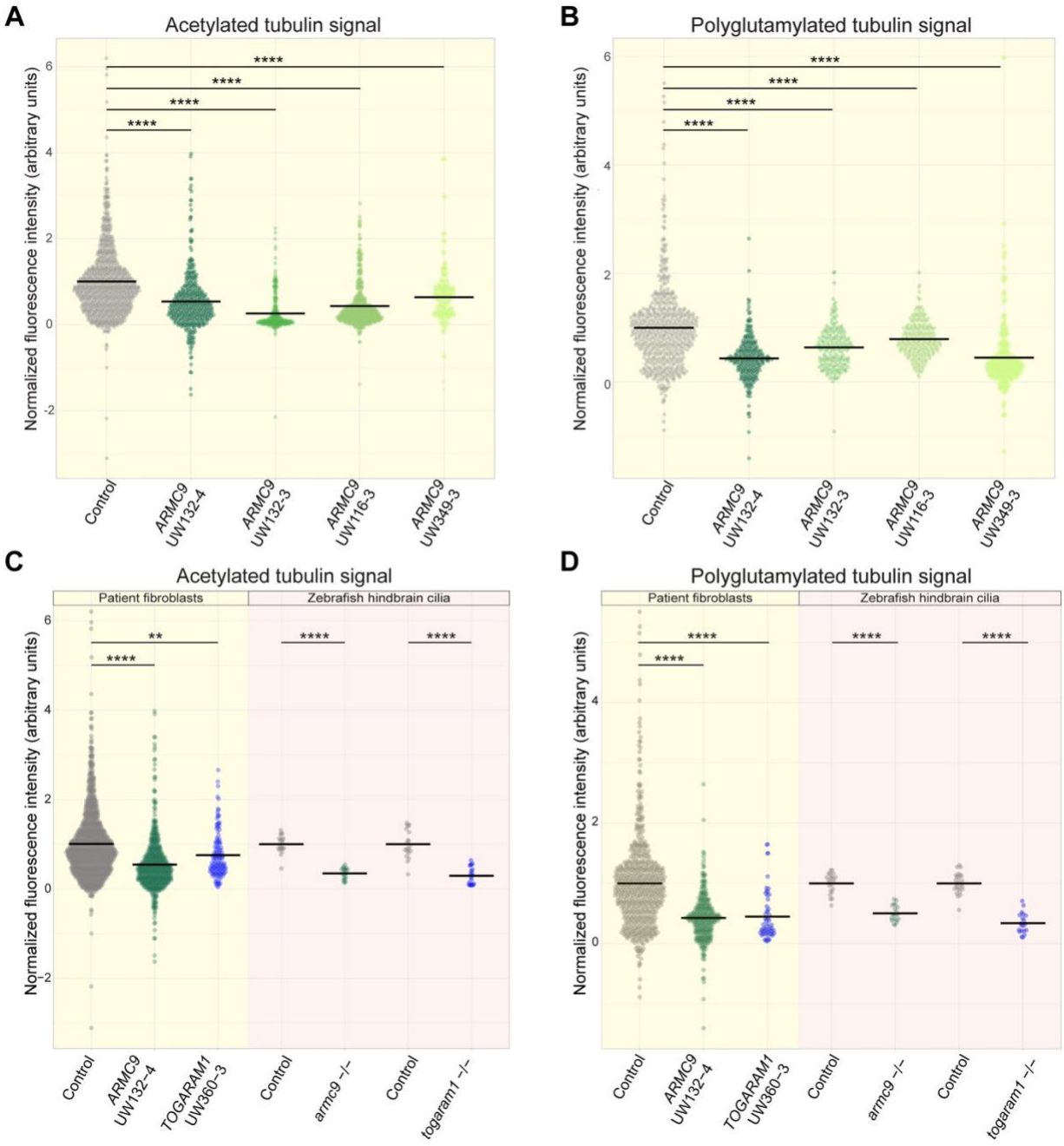

Supplemental Figure 10 Aberrant post-translational modifications across *ARMC9* patient fibroblast lines. **(A)** Normalized acetylated alpha-tubulin fluorescence intensity in control and *ARMC9* patient fibroblasts. >80 cilia were assessed per line for measurements. (control = 848 cilia, UW132-4 = 397 cilia, UW132-3 = 258 cilia, UW116-3= 399 cilia, and UW349-3= 84 cilia). p<0.0001 between control and patient cilia using one-way ANOVA and Dunnett's multiple comparison test. **(B)** Normalized polyglutamylated tubulin fluorescence intensity in control and *ARMC9* patient fibroblasts. >150 cilia were assessed per line for measurements. (control = 557 cilia, UW132-4 = 262 cilia, UW132-3 = 179 cilia, UW116-3= 253 cilia, and UW349-3= 194 cilia). p<0.0001 between control and patient cilia using one-way ANOVA and Dunnett's multiple comparison test. **(C)** Full graphs of the dot plots shown in Figure 7E-F showing all data points. P-value symbols: **p≤0.01, ****, p≤ 0.0001. Bars represent the mean.

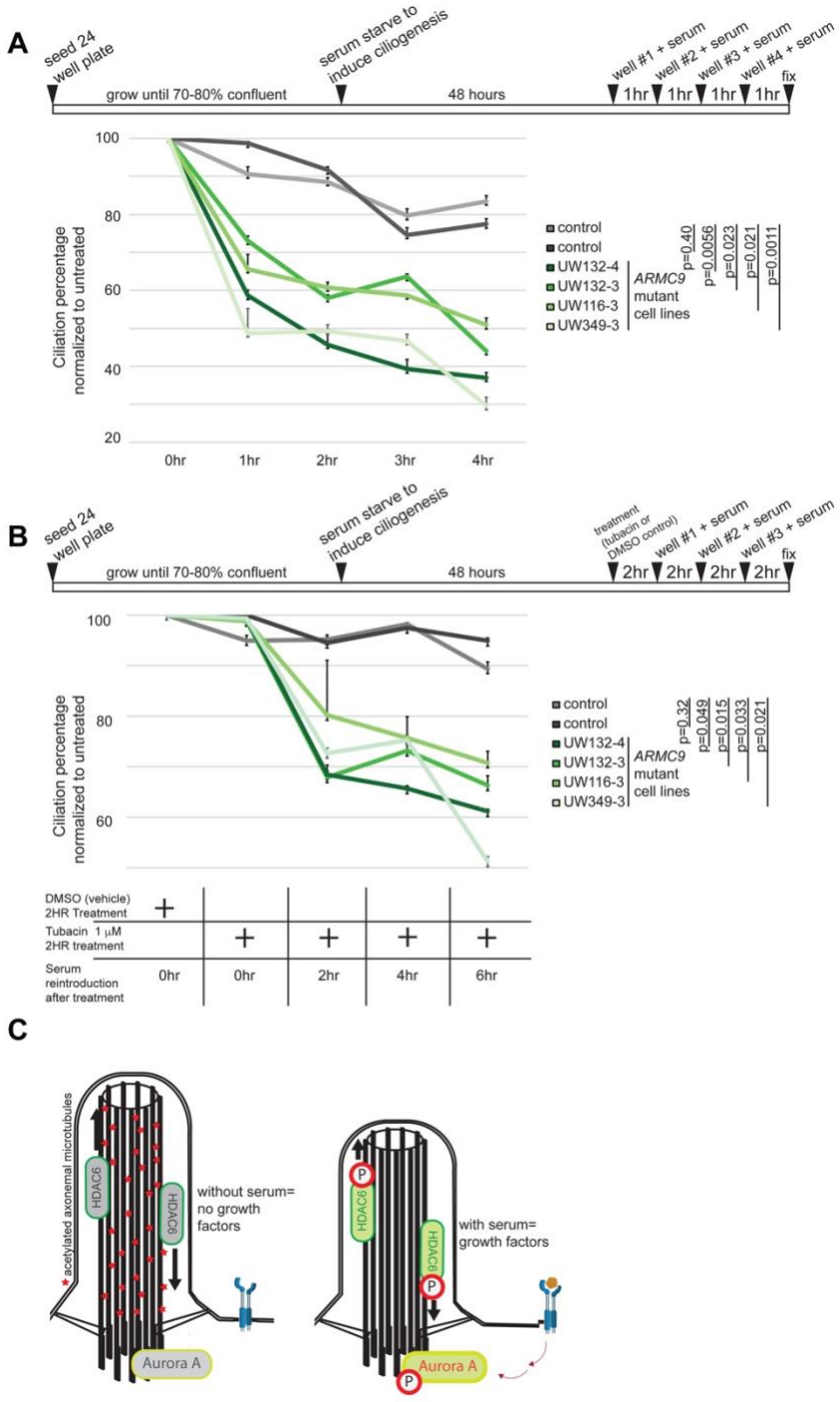

Supplemental Figure 11 *ARMC9* patient fibroblasts exhibit reduced cilium stability. **(A)** Serum readdition assay schematic and time course showing ciliation percentages normalized to serum-starved cells for each cell line. Note accelerated loss of cilia in all *ARMC9* lines. **(B)** Serum readdition assay schematic with HDAC6 inhibitor (Tubacin) treatment to block HDAC6 activity (to test whether the faster resorption observed in ARMC9 lines observed in A is caused by overactive deacetylation) and time course showing ciliation percentages normalized to vehicle-treated serum-starved cells for each cell line. For (A) and (B), error bars represent 95% confidence intervals and Student's t-test with unequal variance was used to test for

differences in slope modeled by linear regression. Note that HDAC6-inhibition does not rescue the accelerated loss of cilia in *ARMC9* lines, but does inhibit resorption in controls. **(C)** Schematic model of HDAC6 activity in ciliary disassembly. Upon initiation of resorption, histone deacetylase 6 (HDAC6) becomes activated and deacetylates ciliary microtubules, a required step for resorption.

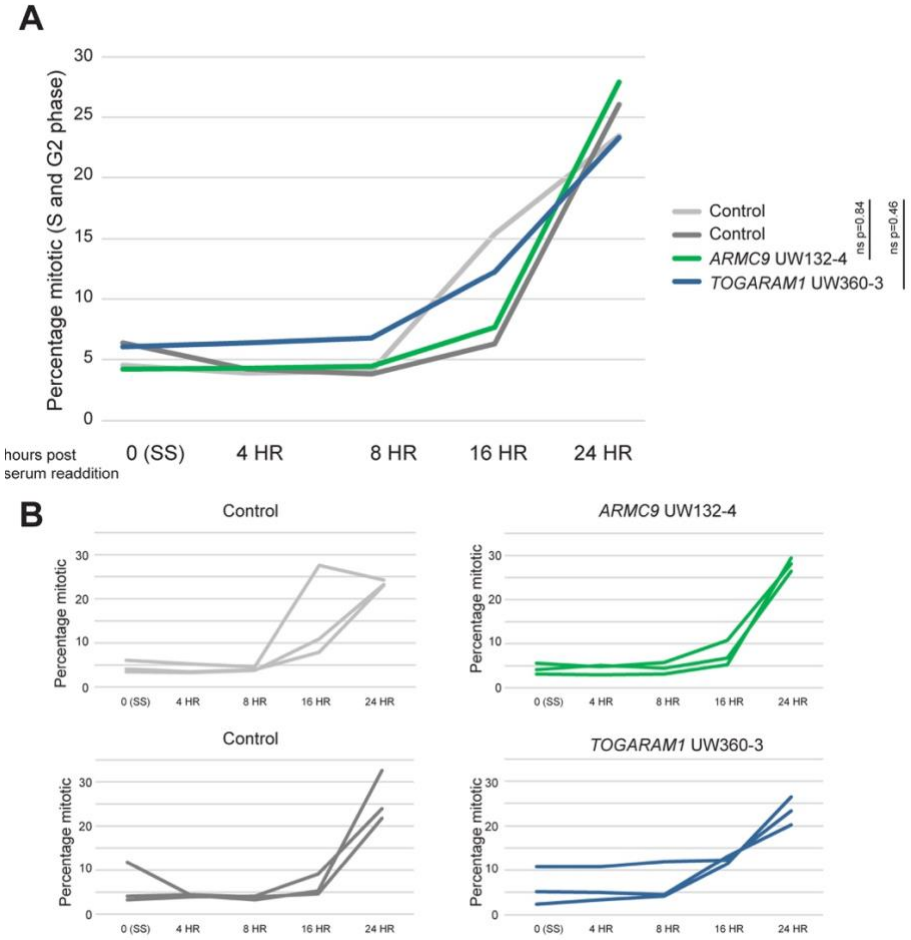

Supplemental Figure 12 *ARMC9* and *TOGARAM1* patient fibroblasts cells reenter the cell cycle normally after serum readdition. **(A)** Average of three experiments assessing cell cycle stage after serum readdition. 10,000 DAPI-stained nuclei were assessed at each time point by flow cytometry. **(B)** Individual experiments for each cell line.

University of Washington Center for Mendelian Genomics (UW-CMG)
Michael J. Bamshad[1,2]; Suzanne M. Leal[3]; and Deborah A. Nickerson[1]; Peter Anderson[1]; Tamara J. Bacus[1]; Elizabeth E. Blue[1]; Kati J. Buckingham[1]; Jessica X. Chong[1]; Colleen P. Davis[1]; Christopher Frazar[1]; Danielle Giroux[1]; William W. Gordon[1]; Martha Horike-Pyne[1]; Jameson R. Hurless[1]; Gail P. Jarvik[1]; Eric Johanson[1]; Tom Kolar[1]; Melissa P. MacMillan[1]; Colby T. Marvin[1]; Sean McGee[1]; Daniel J. McGoldrick[1]; Betselote Mekonnen[1]; Patrick M. Nielsen[1]; Karynne Patterson[1]; Ben Pelle[1]; Aparna Radhakrishnan[1]; Matthew A. Richardson[1]; Peggy D. Robertson[1]; Erica L. Ryke[1]; Aimee M. Schantz[1]; Isabelle Schrauwen[3]; Kathryn M. Shively[1]; Joshua D. Smith[1]; Monica Tackett[1]; Machiko S. Threlkeld[1]; Marc Wegener[1]; Jeffrey M. Weiss[1]; Marsha M. Wheeler[1]; Janson J. White[1]; Qian Yi[1]; Di Zhang[3]; and Xiaohong Zhang[1]

1. University of Washington, Seattle, Washington, USA
2. Seattle Children's Hospital, Seattle, Washington, USA
3. Columbia University, New York City, New York, USA

Genomics England Research Consortium
Ambrose, J. C. [1]; Arumugam, P.[1]; Baple, E. L. [1]; Bleda, M. [1]; Boardman-Pretty, F. [1,2]; Boissiere, J. M. [1]; Boustred, C. R. [1]; Brittain, H.[1]; Caulfield, M. J.[1,2]; Chan, G. C. [1]; Craig, C. E. H. [1]; Daugherty, L. C. [1]; de Burca, A. [1]; Devereau, A. [1]; Elgar, G. [1,2]; Foulger, R. E. [1]; Fowler, T. [1]; Furió-Tarí, P. [1]; Hackett, J. M. [1]; Halai, D. [1]; Hamblin, A.[1]; Henderson, S.[1,2]; Holman, J. E. [1]; Hubbard, T. J. P. [1]; Ibáñez, K.[1,2]; Jackson, R. [1]; Jones, L. J. [1,2]; Kasperaviciute, D. [1,2]; Kayikci, M. [1]; Kousathanas, A. [1]; Lahnstein, L. [1]; Lawson, K. [1]; Leigh, S. E. A. [1]; Leong, I. U. S. [1]; Lopez, F. J. [1]; Maleady-Crowe, F. [1]; Mason, J. [1]; McDonagh, E. M. [1,2]; Moutsianas, L. [1,2]; Mueller, M. [1,2]; Murugaesu, N. [1]; Need, A. C. [1,2]; Odhams, C. A. [1]; Patch, C. [1,2]; Perez-Gil, D. [1]; Pereira, M. B.[1]; Polychronopoulos, D. [1]; Pullinger, J. [1]; Rahim, T. [1]; Rendon, A. [1]; Riesgo-Ferreiro, P.[1]; Rogers, T. [1]; Ryten, M. [1]; Savage, K. [1]; Sawant, K. [1]; Scott, R. H. [1]; Siddiq, A. [1]; Sieghart, A. [1]; Smedley, D. [1,2]; Smith, K. R. [1,2]; Smith, C. S. [1]; Sosinsky, A. [1,2]; Spooner, W. [1]; Stevens, H. E. [1]; Stuckey, A. [1]; Sultana, R. [1]; Thomas, E. R. A. [1,2]; Thompson, S. R. [1]; Tregidgo, C. [1]; Tucci, A. [1,2]; Walsh, E. [1]; Watters, S. A. [1]; Welland, M. J. [1]; Williams, E. [1]; Witkowska, K. [1,2]; Wood, S. M. [1,2]; Zarowiecki, M.[1]

1. Genomics England, London, UK
2. William Harvey Research Institute, Queen Mary University of London, London, UK.

Full uncut gels and blots

Figure 1F

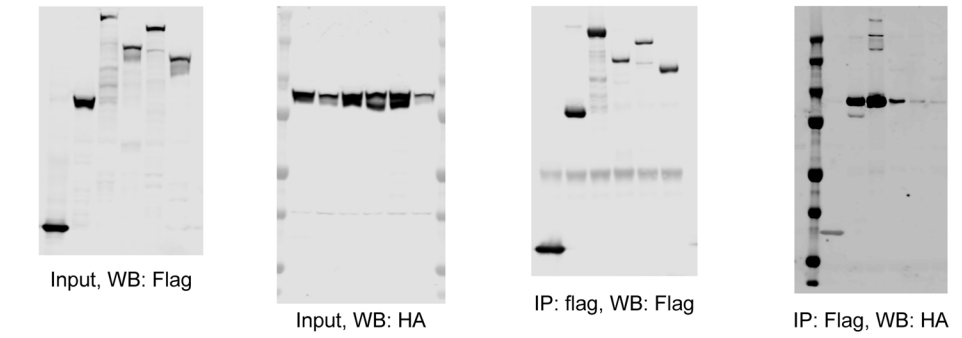

Figure 1H

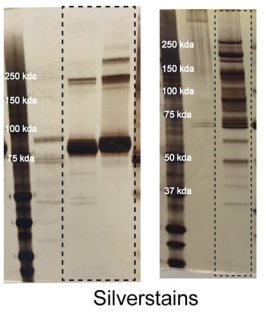

Figure 3G

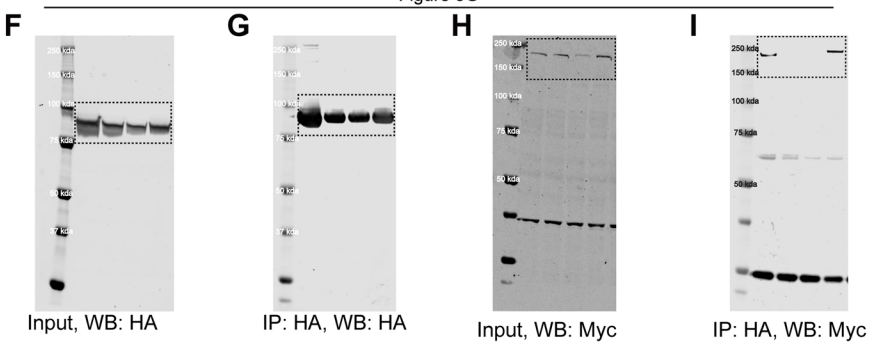

Figure 6C & 7A

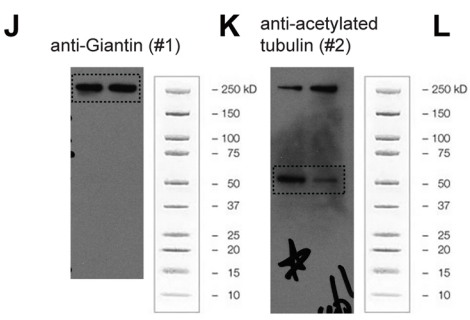

Figure 6 C & D

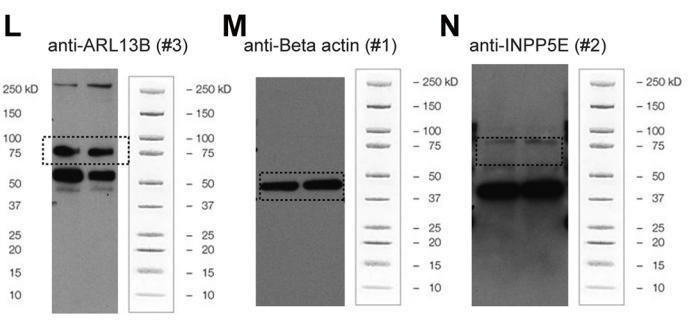

Figure 7B

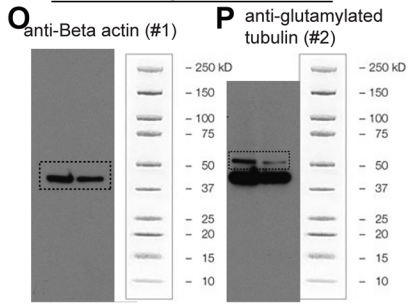

Figure 5A

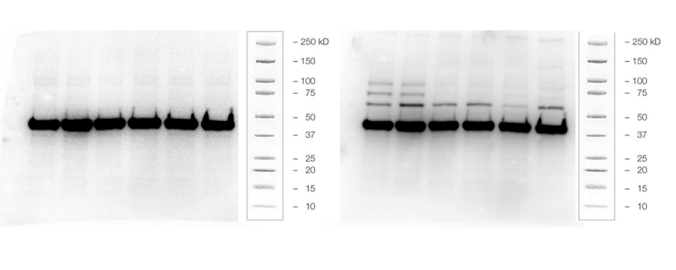

Supplemental figure 1

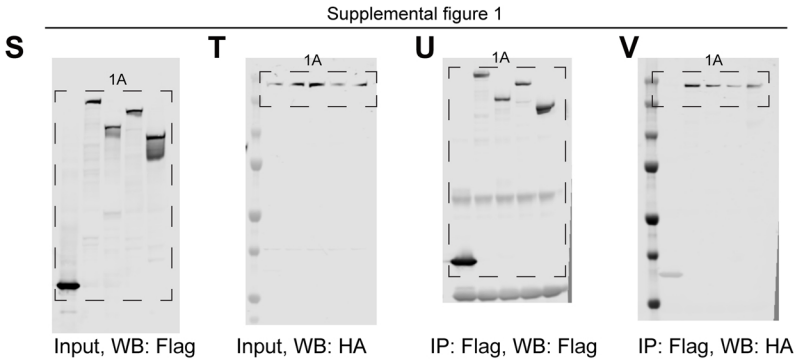

Supplemental figure 1

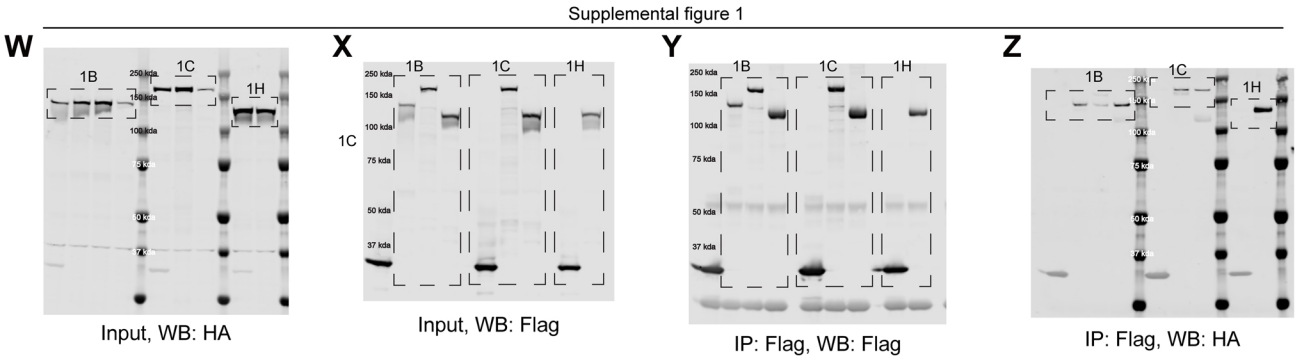

Supplemental figure 1

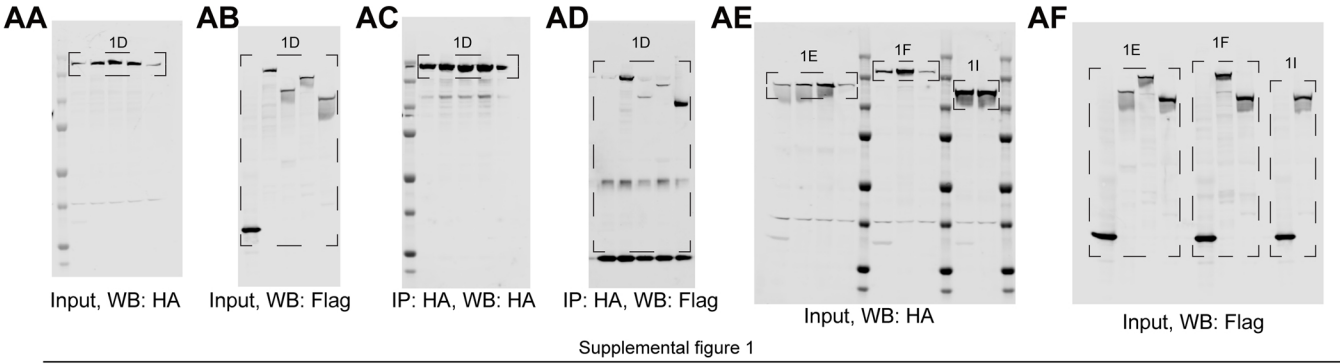

Supplemental figure 1